journal

Alumina

J. Am. Ceram. Soc., 86 [4] 612–22 (2003)

Structure of Sapphire Bicrystal Boundaries Produced by Liquid-Phase Sintering

Bernard J. Hockey, Sheldon M. Wiederhorn,* John E. Blendell,* Jong-Sook Lee, and Myung-Koo Kang

National Institute of Standards and Technology, Gaithersburg, Maryland 20899-8500

The structure and composition of sapphire bicrystal boundaries produced by liquid-phase sintering depended on the crystallographic misorientation of the crystals across the boundary and on the orientation of the boundary. Basal twist boundaries of 15° or 30° were not wetted by glass, but contained significant amounts of Ca and Si at the boundary. For tilt boundaries of 7° or 12°, the glass wetted segments of boundaries that contained the basal plane of either crystal. Boundary segments with orientations of 40° or more from the basal plane, however, were dewetted (i.e., "dry"). Boundary segments oriented less than ~40° from the basal orientation were partially wetted, consisting of segments of wetted and dry grain boundaries. For the 12° tilt boundary, Ca and Si could be detected on portions of the boundary that contained no glass. For bicrystal boundaries having tilts of ≤4°, dewetting occurred for all observed boundary orientations. Basal-oriented segments in these small angle tilt boundaries contained noticeable concentrations of adsorbed Ca and Si, while nonbasal segments were apparently free of Ca and Si. Most results could be explained based on a combined Wulff plot construction, which predicts partially wetted grain boundaries and "missing" angles for unwetted grain boundaries. Results that could not be explained by the construction included growth step ledges bounded by nonequilibrium facet planes.

I. Introduction

A NUMBER of studies have been conducted to characterize glass-containing grain boundaries in aluminum oxide. Several characterized the structure of grain boundaries in commercial grades of aluminum oxide using transmission electron microscopy.[1–4] Almost all grain boundaries examined were wetted by glass and were facetted, on the (0001) basal plane and on $\{01\bar{1}2\}$, $\{10\bar{1}1\}$, $\{11\bar{2}0\}$ and $\{11\bar{2}3\}$ planes. These are low-energy, equilibrium planes for α-Al_2O_3.[5] Occasionally, boundaries that appeared to be unwetted by a glass phase were also observed,[1,2] but these were assumed to be special boundaries, such as twin boundaries, and were not characterized further.

Flaitz and Pask[6] and Shaw and Duncombe[7] showed that glass-free aluminum oxide grain boundaries could be penetrated by glass fully saturated in aluminum oxide. Flaitz and Pask placed a drop of such glass on the surface of polished aluminum oxide specimens made without glass-forming sintering aids. After heat treatment, they observed swelling of the penetrated region and facetting of the aluminum oxide grains within the penetrated region. Shaw and Duncombe obtained similar results by placing densely sintered, glass-free, aluminum oxide samples into molten glass saturated with aluminum oxide. The glass penetrated the grain boundaries, forcing the grains apart and resulting in facetted grains. After penetration, many of the grains were isolated from one another by distances larger than the average grain size of the resultant material, which also coarsened during the procedure. Approximately 16% of the grains remained bonded after penetration, suggesting the existence of boundary conditions for which grain boundary penetration did not occur. In neither study, however, were the boundary conditions associated with penetration explored. Kim *et al.*[8] investigated the stability of a calcium–aluminum–silicate film between two surfaces of sapphire with near-basal orientations. Bicrystals were made by the growth of two sapphire plates through a vitreous-bonded alumina tape so that the misorientation across the boundary was constant for all orientations of the grain-boundary that separated the crystals. The growth process consumed the aluminum oxide grains in the tape, creating a bicrystal with a boundary that was in chemical equilibrium with any glass left at the boundary.

The structure of the grain boundary produced by Kim *et al.*[8] depended on both the crystal misorientation, θ, across the boundary and the relative grain boundary orientation, ϕ. For their particular boundary, the misorientation, θ, was largely defined by a 7° rotation about the near common $[10\bar{1}0]$ direction (the ***m***-direction), and boundary orientations, ϕ, measured relative to the median ***c***-axis of roughly ±40°. Regions of the boundary that lay close to the basal plane orientation were completely wetted by glass and fully faceted. For boundary orientations inclined to the basal orientation by angles, ϕ, greater than about 38°, the boundary was completely dry, i.e., devoid of detectable glass, and exhibited dislocation contrast. At intermediate angles, $\phi \sim 7°$ to 38°, the boundary was partially wetted, consisting of segments that contained the glassy phase separated by segments of dislocation boundary. The formation of these three types of boundary structures along the same boundary was qualitatively explained by comparing the energy of a fully wetted boundary with the energy of a dry, small-angle dislocation boundary. Blendell, Carter, and Handwerker expanded the two-dimensional energy analysis to three dimensions.[9]

The data of Kim *et al.*[8] are limited, being based on one bicrystal boundary misorientation over limited boundary orientations. In the current study, we extend the database to other misorientations, with experimental results obtained from a broader range of boundary orientations. By so doing, we intended to test theoretical predictions[8] concerning the range of wetting for low angle boundaries and the kind of grain boundary structure expected for higher angle boundaries. Based on the earlier study,[8] we predicted that grain boundary misorientations less than about $\theta = 4°$ would be dry for all values of ϕ, and so we selected orientations to test this prediction. In addition, we explored the structure of grain boundaries with larger values of θ than that studied by Kim[8] to determine whether the same partially wetted structures would be seen on these boundaries. The possibility of wetted boundaries for basal grain boundaries, $\phi = 0°$, was also explored. Although the current results support the energy-based theory of grain boundary structure,[8,9] they also describe other elements that are seen to be

A. H. Heuer—contributing editor

Manuscript No. 186775. Received August 15, 2002; approved December 9, 2002.
Presented at the International Symposium on Science and Technology of Alumina (Schloss-Ringberg, Germany, March 17–22, 2002).
*Member, American Ceramic Society.

important in determining grain boundary structure. Strong adsorption of Ca and Si to basal planes modifies the structure of "dry" grain boundaries situated on the basal plane. Also, nonequilibrium growth facets/ledges are observed, and the interactions of these growth structures appear to be important to boundary formation and resultant structure. Finally, the number of dry boundaries seen in the present set of experiments seems to be more than would be expected from previous polycrystalline observations. Whether this represents a change in the distribution of grain boundary types or a change in the wetting behavior is not known.

II. Experimental Procedure

Normally, five degrees of freedom are required to define a grain boundary. Three angles define the orientation of one crystal with regard to the other, while two angles define the orientation of the boundary. In our study, the intention was to design bicrystal boundaries having misorientations described solely by rotations about a common, specific crystallographic direction, either the [0001] ***c***-axis or the $\langle 11\bar{2}0\rangle$ ***a***-axes. The specific direction of crystal growth was chosen to provide a broad range of boundary orientations for a fixed bicrystal misorientation. As both conventional and high-resolution transmission electron microscopy (TEM) were required to characterize the bicrystal boundaries, the boundary orientation could only be defined in terms of its projection in the cross-sectional plane of observation. For these reasons, the bicrystal boundaries are defined in a two-dimensional framework. Here, it is important to note that the boundary misorientation could not be confined to a simple rotation (or tilt) about a specific direction as intended, but also contains minor components which are described in the specific results.

Following this simple boundary description, two distinctly different types of bicrystals were made (Table I). The first was produced by the directed growth of two ***c***-axis-oriented plates which had been rotated by ~15° or 30° about their near common ***c***-axis to create basal twist boundaries. The second type of bicrystal was designed to create tilt boundaries with tilt misorientations, θ, of ~2°, 3°, 4°, 7°, and 12°. For θ = 3°, 7°, and 12°, the tilts were associated with an angular rotation about a common $[11\bar{2}0]$, ***a***-axis, using either ***c***-axis-directed growth (θ = 3° and 7°) or ***m***-axis-directed growth (θ = 12°). The θ = 4° tilt boundary was made by ***m***-directed growth by rotation about the ***m***-axis, while the θ ~ 2° boundary was made by ***a***-directed growth by rotation about the ***m***-axis. TEM observations on basal boundaries from ***c***- or ***m***-growth were primarily made on cross sections cut normal to the ***a***-axis of rotation; for ***a***-growth bicrystals, cross sections were cut normal to the ***m***-axis. Observations on basal twist boundaries were made normal to an ***a***-axis in one of the crystals that constitute the bicrystal. Conventional TEM examination was primarily conducted at 300 kV on a Philips 430, equipped with EDS and high-resolution studies were conducted at 297 kV on a JEOL 3010, equipped with EDS and a Gatan image filter (GIF).† Table I provides a summary description of the bicrystal boundaries examined in this study.

A schematic of the bicrystal fabrication process[8] is shown in Fig. 1. A pair of crystallographically oriented plates was cut from a sapphire rod. For bicrystals having a basal tilt misorientation of θ, the surfaces of each plate were then ground at an equal but opposite angle of (½)θ along the same crystallographic direction. The plates were then used to form a sandwich with a tape of alumina containing anorthite ($CaAl_2Si_2O_8$) glass between them. This procedure was used to produce tilt boundaries by ***c***-, ***a***-, and ***m***-directed growth. Basal twist boundaries were made by rotating two basal plates by a prescribed angle about the ***c***-axis. In all cases, the boundary orientation, φ, is measured relative to the median ***c***-direction for the bicrystal, regardless of the growth direction (Figs. 1(b) and (c)).

Experimentally, the sapphire plates and alumina tape were pressed together using an applied pressure of ≈10 MPa at 1600°C. The single crystals grew through the alumina tape from both sides to form a bicrystal with a boundary containing some residual glassy phase. The boundaries so formed were stationary when all of the grains in the alumina tape were consumed. They were not flat, but rough, and even after annealing the bicrystals (stress-free) for periods of 200 h or 400 h at 1600°C or 200 h at 1800°C, they retained their roughness. Over distances ranging from 10 nm to 1 μm, however, the boundaries exhibited local features that depended on the tilt misorientation, θ, and the boundary orientation, φ, of the bicrystal. These features are believed to be the equilibrium structure of a bicrystal having the same orientation, θ and φ. In all cases, the bicrystal boundaries were examined in cross section from specimens cut normal to the direction of growth.

III. Results

(1) Formation of Sapphire Bicrystals

The growth of the sapphire crystals through the alumina tape is illustrated in Figs. 2(a–d). As expected from the results of Finkelstein *et al.*,[4] the growth rate and the morphology of the

†Certain commercial equipment, instruments, or materials are identified in this paper in order to specify the experimental procedure adequately. Such identification is not intended to imply recommendation or endorsement by the National Institute of Standards and Technology, nor is it intended to imply that the materials or equipment identified are necessarily the best available for the purpose.

Table I. Description of the Bicrystal Boundaries Examined†

Rotation axis	Rotation angle, θ (deg)	Sapphire surface	Boundary type	Boundary angle, φ (deg)	Condition of boundary
c [0001]	15, 27	~(0001)	Twist	0	Dry, detectable Si and Ca at boundary (Fig. 12)
m $[10\bar{1}0]$	~2	~$(1\bar{2}10)$	Tilt	±45 to 90	Dry, *no* detectable Si or Ca at boundary
a $[1\bar{2}10]$	<3	~(0001)	Tilt	±1.5	Dry, detectable Ca and Si at boundary, trapped glass pockets (Figs. 9–11)
m $[10\bar{1}0]$	~4	~$(10\bar{1}0)$	Tilt	±45 to 90	Dry, some small glass pockets at boundary, *no* detectable Si or Ca at boundary (Figs. 3, 4)
m $[10\bar{1}0]$	~7	~3.5° to (0001)	Tilt	±3.5 to ±40	±3.5°, fully wetted boundaries;[8] >3.5° to 38°, partially wetted boundaries;[8] >38°, dry boundary[8]
a $[1\bar{2}10]$	~7	~3.5° to (0001)	Tilt	±3.5	±3.5°, fully wetted boundaries (hard to detect glass on some boundaries, but high Si and Ca content, Fig. 7)
a $[1\bar{2}10]$	~12	~6° to $(10\bar{1}0)$	Tilt	0 to ±90	±6°, fully wetted boundaries; 6° to 40°, partially wetted boundaries; ±40°, dry, detectable Ca and Si at boundary (Figs. 5, 6)

†"Sapphire surface" gives the surface orientation of the sapphire plates used to make the bicrystal. Boundary angle, φ, gives the orientation of the boundary normal relative to the median ***c*** [0001] direction. The 7° tilt boundary information includes results from Kim *et al.*[8]

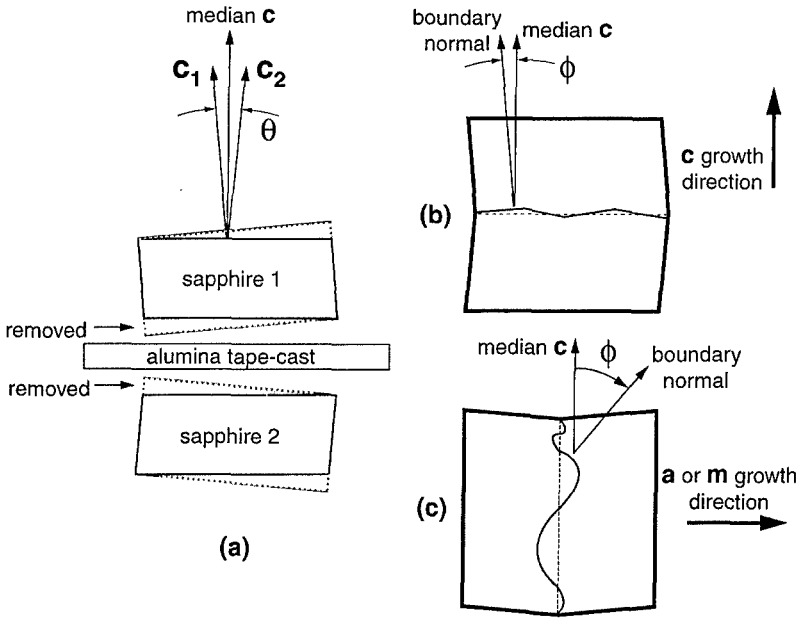

Fig. 1. Schematic diagram of the procedure for making sapphire bicrystals: (a) the orientation of the two plates of sapphire is shown relative to the slip-cast glass–aluminum oxide tape. (b) The growth direction is equal to the median ***c***-direction for ***c***-growth bicrystals. The boundaries tend to be flatter for this growth direction. (c) For growth in the ***a***- or ***m***-direction, the boundary tends to be wavy. The median ***c***-direction and the ***a***- or ***m***-direction are at right angles to each other. The normal to the grain boundary is measured relative to the median ***c***-direction.

growth interface depended on the orientation of the migrating sapphire surface. This dependence on orientation during bicrystal formation also affected the morphology of the bicrystal boundary. As seen in Figs. 2(a) and (b), the growth of ***a***-axis- or ***m***-axis-oriented sapphire plates proceeded irregularly, resulting in a wavy growth interface during migration (Fig. 2(a)) and a wavy bicrystal boundary (Fig. 2(b)). For these prismatic directions, growth occurs more rapidly than ***c***-axis growth,[4] but is variable, depending on local conditions, such as the orientation of opposing grains and the size (thickness) of accumulated intergranular glass phase. As a consequence of these local variations in migration rate, the growth front assumes an irregular shape. Sometimes, nearly encapsulated grains are present along the growth front. In addition, fully encapsulated glass channels, elongated in the growth direction, are

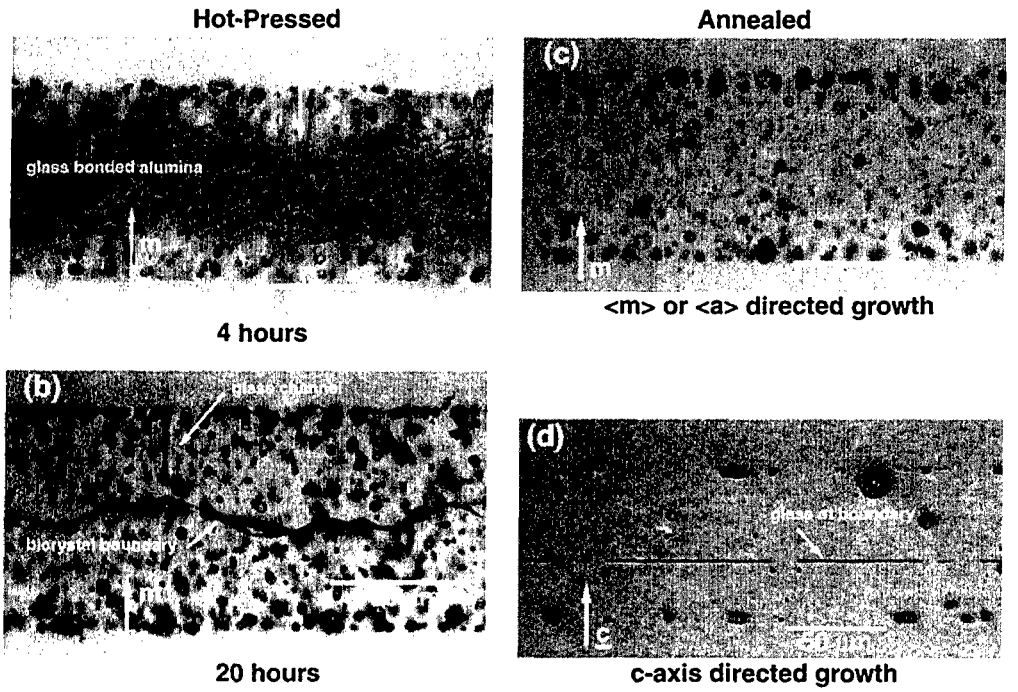

Fig. 2. Various stages of bicrystal boundary formation by directed growth of sapphire through glass bonded alumina at 1600°C. (a) Early stage growth of the bounding sapphire plates into the glass-bonded alumina. Encapsulated pores, many of which contain glass, mark the region of intergrowth. (b) Final stage of directed growth under an applied pressure. All of the grains from the original tape-cast alumina have been consumed and the sapphire halves are separated by a single boundary containing a glass interphase. For ***a***- and ***m***-growth directions, the boundary is wavy. An arrow shows the presence of encapsulated glass-filled channels. (c) The final stage of ***m***- or ***a***-axis growth shows that the boundary loses optical visibility. (d) In the final stage of ***c***-axis growth, the planar boundary is defined by entrapped interfacial glass.

formed in the wake of the boundary (Fig. 2(b)). After annealing, neither encapsulated glass channels nor accumulated interfacial glass can be found near the bicrystal boundary (Fig. 2(c)). Instead, the residual glass is contained within pores distributed in the region of intergrowth. The wavy morphology of bicrystal boundaries produced by ***a***- or ***m***-axis-directed growth offered a particular advantage, as a wide range of boundary orientations about these growth directions could usually be examined within a single sample.

In contrast to growth in the ***a***- or ***m***-direction, growth of ***c***-axis-oriented crystals occurs along a nearly planar growth front and, consequently, results in a relatively planar bicrystal boundary (Fig. 2(d)). As will be shown, boundaries formed by ***c***-axis growth with misorientations, θ, of 3° to 7° across the boundary can be described as stepped, with flat basal-oriented segments displaced along the direction of growth. Observed normal displacements of the planar basal segments ranged in size from less than 1 nm to several micrometers. For the larger size displacements, the planar segments are joined by dislocation boundary segments or by thin, plate-shaped glass pockets, encapsulated at the boundary (Fig. 2(d)).

(2) Bicrystal Boundaries Formed by m and a Growth

Despite the wavy morphology of bicrystal boundaries produced by ***m***- or ***a***-axis growth, a relatively broad range of boundary orientations about the mean growth direction could be examined by TEM. Figure 3, for example, illustrates the change in boundary orientation with distance along the boundary for a small angle (4° basal tilt) bicrystal boundary produced by ***m***-axis growth. Two segments of the same boundary separated by a distance of roughly 10 μm are shown in cross section. Both images were obtained under the same diffraction conditions (insert to Fig. 3) after translation, and it can be seen that both the trace of the boundary and its inclination to the foil have changed. More generally, the boundary orientation, ϕ, gradually changed along its trace. Although each boundary segment appears planar on this scale, no preference for particular crystallographic planes, including the $\{10\bar{1}0\}$ growth plane, was found. Figure 3 also shows that this boundary, whose misorientation corresponds to a 4° rotation about the ***m***-axis of growth and $\leq 1°$ about the ***c***-axis, is characterized only by dislocation and/or thickness fringe contrast. No evidence was found for a glassy interphase, regardless of boundary orientation. Occasionally, however, pores containing residual glass were found along the boundary (Figs. 4(a) and (b)). Such glass-filled pores appear to be encapsulated, since no evidence for glass, or more specifically Si and/or Ca from the anorthite glass phase, could be detected by EDS, either at any point along the boundary or in regions adjacent to the glass-filled pores (Fig. 4(c)). A similar description of boundary morphology, boundary contrast, and boundary composition (specifically, the absence of detectable glass) applies to small misorientation ($\leq 2°$) boundaries produced by ***a***-axis growth. Although ***a***-plane boundary segments normal to the direction of growth were found, they exhibited no distinguishing features or compositional differences.

TEM results from a bicrystal boundary having a much larger misorientation are summarized in Figs. 5 and 6. For this boundary, the misorientation across the boundary corresponds to a 12° rotation about the ***a***-direction, and the direction of growth was along the median ***m***-direction. Here, care was taken to maintain the arbitrarily defined sense of ***m*** so that the deviation of ***m*** across the boundary was $\pm 6°$ not $\pi \pm 6°$. The representative images of the same boundary in Figs. 5 and 6 are cross-sectional, viewed roughly along the ***a***-axis. Under these growth conditions, the bicrystal boundary orientation deviated by 90°, so those boundary segments having orientations ranging from near the median ***m***-direction of growth (Fig. 5(a)) to the median ***c***-direction of growth (Figs. 5(b) and 6) could be examined. For boundary orientations ranging from the median ***m***, to roughly 30° from the median ***c***, the boundary was

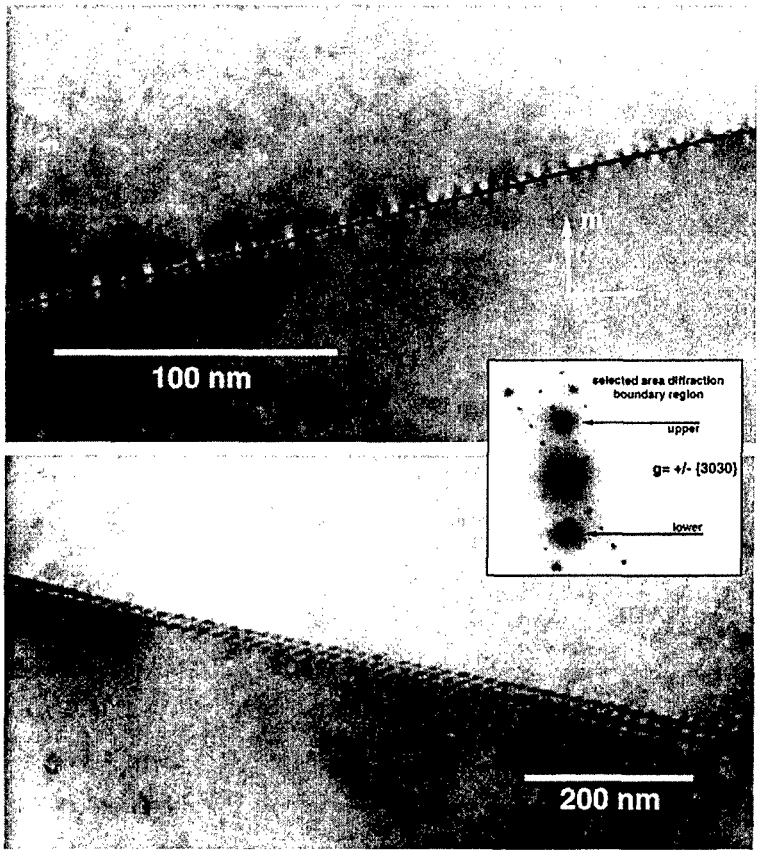

Fig. 3. Small angle ($\theta = 4°$) bicrystal boundary formed by directed ***m***-axis growth. By TEM, the boundary was found to gradually change orientation and to exhibit dislocation and/or thickness fringe contrast. No evidence was found for a glassy interphase or for Si and Ca adsorbates from the glass phase. Similar results apply to small angle bicrystal boundaries produced by ***a***-axis growth.

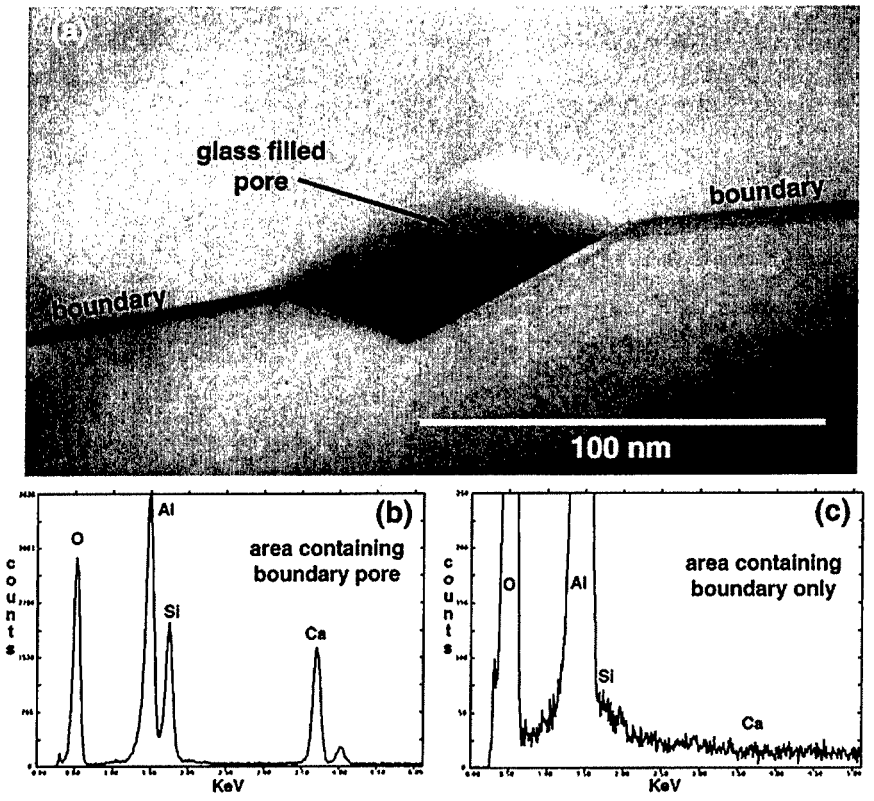

Fig. 4. (a) TEM micrograph of a glass-filled pore intersected by the boundary shown in Fig. 3. Using EDS, the glass phase is found only at the pore (b), and not within adjacent boundary regions (c).

distinguished only by typical grain boundary contrast (thickness fringe contrast). No evidence for a discrete glassy interphase or accumulated glass was found in this range of boundary orientations, even where the boundary plane coincided with the specific $\{01\bar{1}2\}$ rhombohedral twin plane (***r***) normal to the ***a***-axis of rotation (Fig. 5(c)). Nevertheless, EDS spectra obtained from various regions of the boundary typically exhibited the presence of small concentrations of Si and Ca over this entire range of orientations (Fig. 5(d)). Because the residuals for these elements were close to the detection threshold for our EDS systems, no attempt was made to quantify either the Ca/Si concentration ratio or any variation with boundary orientation. From these results, it appears that this 12° boundary has dewetted over most orientations, but has retained detectable concentrations of cations (Si and Ca) from the glass phase during sintering.

In contrast to this dewetted boundary structure, portions of the boundary orientated near the median ***c***-direction contained a relatively thick, contiguous layer of glass (Figs. 5(b) and (e)). As seen in Fig. 5(b), these boundary segments were always bounded on one side (or the other) by a basal plane surface, while the opposing surface is facetted. Boundary orientations within this 12° angular range about the median ***c***-direction were not found. Similarly, the boundary orientation always changed abruptly by at least 30° from the basal-oriented segments. This behavior is illustrated in Fig. 6, where the wetted portion of the boundary is aligned parallel to the basal plane in the top crystal but then abruptly changes to an orientation that is inclined both to the foil (note the fringe contrast) and to the basal orientation. This inclined region of the boundary also contains "basal steps," having the same structure as the larger, wetted basal-oriented regions seen in more detail in Fig. 5(b).

(3) Bicrystal Boundaries Formed by c-Axis Growth

As stated previously, bicrystal boundaries produced by ***c***-axis growth were relatively flat in that they contained planar segments parallel to the basal orientation of one side of the bicrystal. Changes in boundary orientation tended to occur abruptly between adjacent planar segments, as shown in Fig. 7, where the boundary is viewed in cross section roughly along the ***a***-axis of rotation. The misorientation for this boundary corresponds to 7° about "***a***", 3° about "***c***", and ~1° about "***m***". The boundary in this area consists of segments bounded on one side by basal surfaces so that the boundary orientation changes by ±3.5° about the median ***c*** along its length. Other regions of this bicrystal boundary contained a relatively thick residual glassy interphase (Fig. 8). These results are in qualitative agreement with prior work.[8]

The results of the present study, however, differ in that the sapphire surfaces bounding the glass interphase could not be described in terms of known low-energy, facet planes, except for basal plane facets (Figs. 7 and 8). Instead, the bounding surfaces are considered to be basal surfaces containing growth steps/ledges of various sizes. While the presence of nonequilibrium steps or ledges on the sapphire surfaces complicates the description of the boundary, it does indicate the importance of ledge interactions to the formation of the boundary. The role of ledges and their interaction becomes increasingly more important as the total thickness of the boundary decreases. This is seen in Fig. 7(b), which shows, in more detail, a portion of the boundary seen in Fig. 7(a). In Fig. 7(b), striations in the phase contrast image are seen along the boundary within the crystal half whose basal plane is tilted by ~7° to the boundary plane. While the nature of the contrast exhibited by these striations cannot be explained, the presence of such fine striations on the basal planes in sapphire suggests that they represent basal defects (most likely basal stacking faults) that mark the positions of basal ledges during the final stages of boundary formation. Conceivably, these planar defects are stabilized by the presence of adsorbed Si and Ca. Moreover, as also seen in Fig. 7(b), the presence of a contiguous layer of glass is not always apparent within the boundary. Instead, such regions of the boundary appear to contain discrete, isolated glass pockets of nanoscale dimensions, connected by grain boundary segments. By necessity, the grain boundary segments would

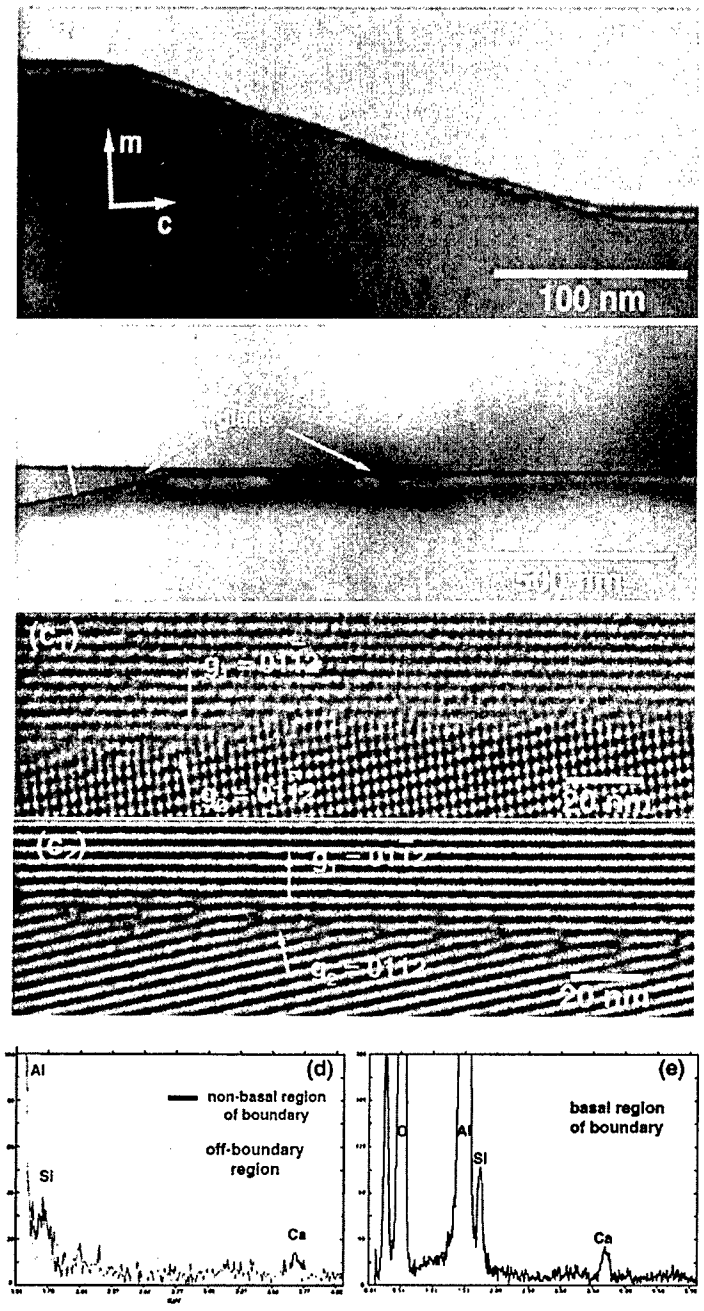

Fig. 5. TEM views of various regions along a large angle ($\theta = 12°$) bicrystal boundary formed by ***m***-axis growth: (a) boundary orientations near the ***m***-growth direction; (b) basal plane boundary region; and (c) $\{01\bar{1}2\}$, rhombohedral twin plane boundary regions. Evidence for a glass interphase was found only in sections of the boundary oriented along the basal orientation in one of the crystal halves (b and e). Nonbasal portions of the boundary contained detectable concentrations of Si and Ca from the glass phase (d).

have to accommodate not only the lattice displacements associated with a 7° basal tilt, but also the stacking disorders and associated charge compensation. As such, the remnant "basal ledge defects" may be stabilized by virtue of being incorporated within the grain boundary defect structure.

Results from a 3° basal tilt boundary are shown in Figs. 9–11, all which are cross-sectional views taken normal to the ***a***-axis of rotation, as indicated in Fig. 9(b). From Fig. 9(a), the boundary consists of relatively large "facetted" pockets of remnant glass elongated along the boundary, together with very narrow, flat boundary segments, designated as "dewetted." The figure overemphasizes the relative extent of glassy boundary compared with the narrow, "dewetted" portions of the boundary, which from Fig. 9(a) appear planar and continuous. In addition, EDS spectra from regions containing these narrow boundaries invariably show the presence of Si and Ca (Fig. 9(c)). As illustrated in Fig. 10, high-resolution, transmission electron microscopic (HREM) examination of these boundary regions provides no definitive evidence for the presence of continuous glassy film having a thickness greater than the linear resolution normal to the basal planes (i.e., one 0006 fringe or 0.2165 nm).

The HREM results in Fig. 10 do show changes in the local contrast both along and normal to the boundary. While the contrast exhibited at the boundary is not understood in detail, the observed changes in contrast normal to the boundary appear related, in part, to changes in the "thickness" of the boundary. The changes in contrast ranged from a pair of basal layers (as indicated in the insert to Fig. 10(b)) to multiple pairs of basal layers, but in no case did they extend beyond one lattice parameter, $|c| = 1.3$ nm. Similarly, relative changes in contrast along the trace of the boundary appear related to small shifts in the boundary position along the ***c***-direction to accommodate slight variations in boundary

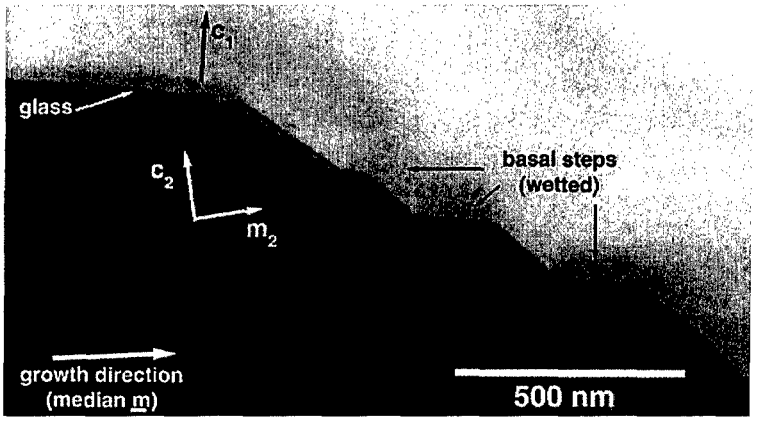

Fig. 6. TEM view illustrating the characteristic, abrupt (~30° to 40°) change in boundary orientation between basal and nonbasal oriented sections of the θ = 12° boundary seen in Fig. 5.

orientation. Here, it is important to note that boundary orientations in the range $\phi = \pm 1.5°$ about the median ***c*** do occur for $\theta \sim 3°$ (Fig. 10(b)). This result is contrary to results on basal boundaries with larger misorientations, such as $\theta = \sim 7°$, where boundary orientations within the range $\phi < \pm 3.5°$ were not observed (Fig. 7(a)). Changes in contrast along the boundary can also be ascribed to sample thickness variations and to changes in orientation, due not only to beam-induced foil buckling, but to residual stresses associated with the dewetted boundary.

Despite all these possible effects, we feel that the observed boundary contrast is primarily related to the presence of defects, such as dislocations and basal stacking faults. These defects are produced to accommodate the lattice distortions and stacking sequence errors that occur when the glassy boundary dewets and the misoriented crystal halves grow together. Clear evidence for complete dewetting along this 3° basal tilt boundary is seen in Fig. 11. In going from right to left along the boundary in Fig. 11(a), the boundary orientation changes abruptly from the near-basal orientation (described above) to a simple dislocation boundary Fig. 11(b) lying roughly 25° to the median basal orientation. Further to the left of this dislocation boundary segment, the boundary is comprised of small, basal segments, which are displaced along the median ***c***-direction and which are separated by small, nanoscale sections of elastically strained, perfect crystal (Fig. 11(c)). In this latter region, all of the defects (dislocations and stacking faults) produced to accommodate the lattice distortions and stacking disorders are concentrated at the small basal segments (Fig. 11(d)). Again, while these small basal segments do exhibit detectable concentrations of Si and Ca by EDS, as in Fig. 9(c), they do not exhibit either isolated pockets of glass or a discernible layer of glass. Accordingly, we consider these basal segments to be extended (both laterally and normally) basal defects, containing relatively high concentrations of Si and Ca adsorbates from the liquid, glassy phase. In this context, neither Si nor Ca was detected along the dislocation boundary or in regions of "perfect" crystal over the range of boundary seen in Fig. 11(a).

Finally, additional observations were made on two basal twist boundaries, produced by a 15° and ~27° rotation of the crystal

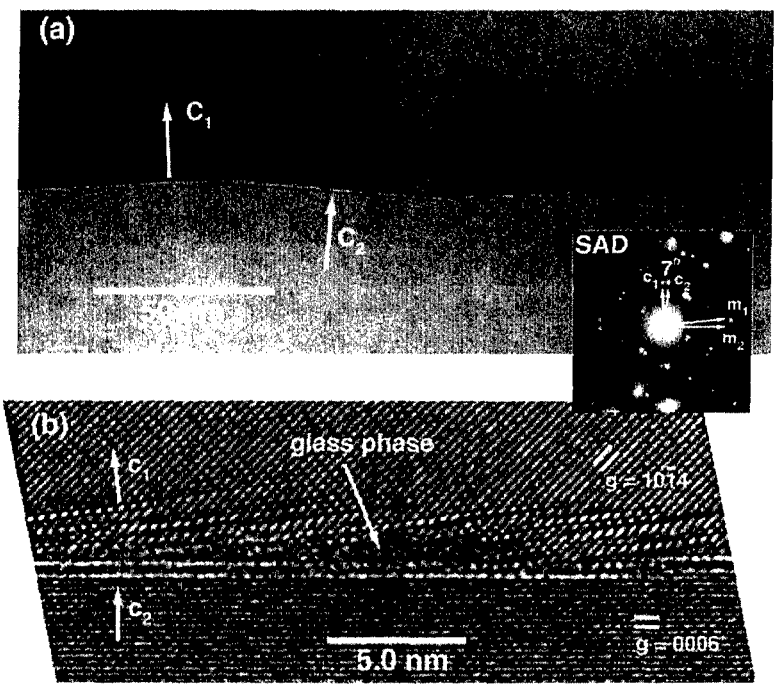

Fig. 7. (a) Large-scale cross-sectional TEM view of a ~7°, basal tilt boundary produced by median ***c***-axis growth. For boundary orientations close to the median ***c***-direction, the boundary assumes a "facetted" structure, such that adjacent "facets" are aligned in an alternating manner along the basal planes of the two crystal halves of the bicrystal. (b) HREM view of a portion of the boundary seen in (a). Evidence for a glassy interphase is only apparent at isolated, nanoscale "pockets" along the boundary.

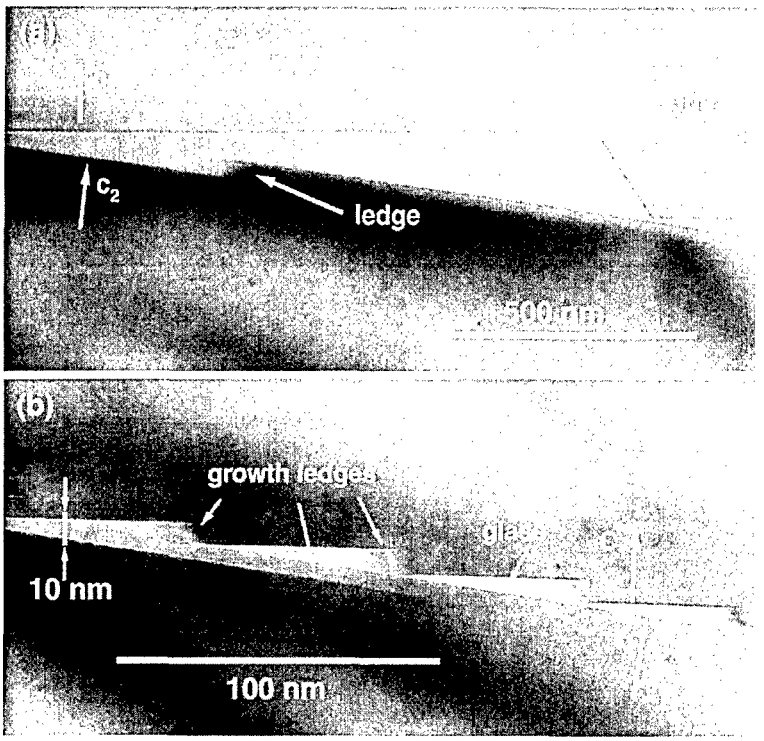

Fig. 8. TEM views of different regions along the ~7° basal tilt boundary seen in Fig. 7. In these regions, the bicrystal boundary contains a thick, contiguous layer of glass. In both cases, the interfacial glass phase is bounded by basal surfaces containing large, growth ledge steps.

halves about their near common *c*-axis. In both cases, the alignment of the basal planes across the boundary was not perfect and the degree of basal tilt was determined to be between 1° to 2°. In general, observations on cross sections cut roughly normal to an *a*-axis of one of the crystals of the bicrystal revealed long (10 μm or more in length) narrow boundary segments along the basal planes separated by relatively large pockets of glass, similar to those seen earlier in Figs. 2(a) and 9(a). Gradual changes in boundary orientation off the near common basal orientation were not observed; instead, displacements of the boundary along the *c*-axis of growth occurred across a glass pocket or across overlapping growth ledges. These growth ledges were typically 10 nm (±5 nm) in height along *c* and were inexplicably always overlapped within the TEM foil.

As illustrated in the representative image shown in Fig. 12, HREM examination of the narrow basal twist boundaries under various diffraction conditions revealed no significant changes in the periodicity of 0006 (d = 0.2165 nm) basal fringes across the boundary due to an interfacial glass film. While changes in image contrast across the boundary are seen, these changes in contrast are typically confined to a width of 1.3 nm or less normal to the boundary. Again, as in the case of basal boundary segments in the 3° basal tilt boundary, both the 15° and ~27° basal twist boundaries were marked by the presence of discernible concentrations of Si and Ca (comparable to that seen in Fig. 9(c)) from the glass phase by EDS.

IV. Discussion of Results

The principal objective of this study was to test the theory developed to rationalize the structure of grain boundaries in

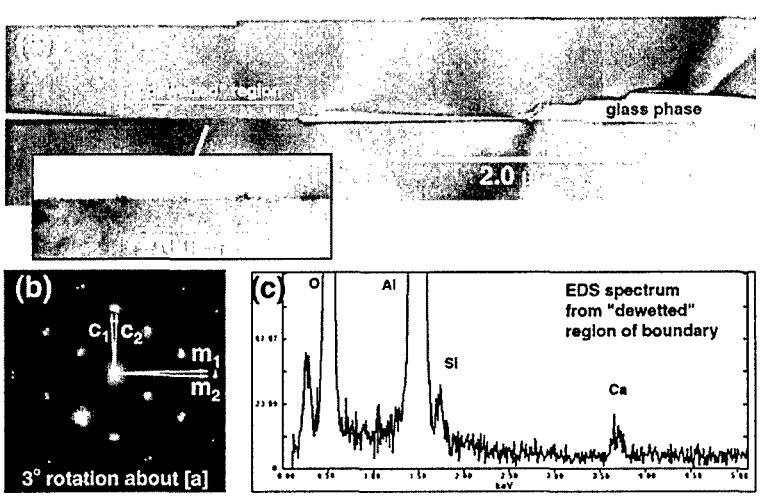

Fig. 9. (a) Large-scale cross-sectional TEM view of a 3° basal tilt boundary viewed along the common *a*-axis of rotation. On this scale, the boundary is seen to consist of narrow, planar segments (designated as "dewetted") separated by interfacial glass pockets elongated along the boundary. (b) Selected area electron diffraction pattern confirming the 3° basal tilt misorientation. (c) Representative EDS spectrum from "dewetted" portion of boundary showing the presence of Si and Ca adsorbates at the boundary.

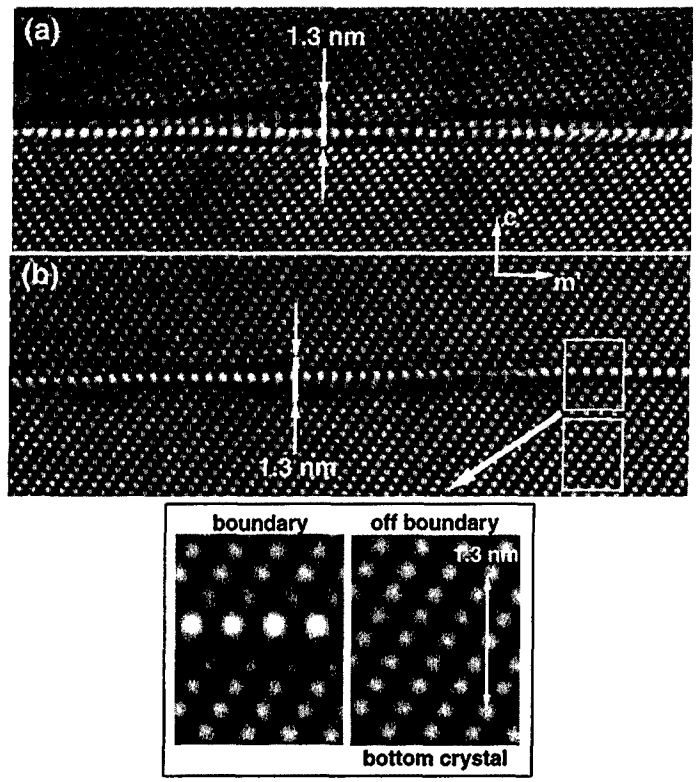

Fig. 10. HREM *a*-axis views of similar, narrow basal boundary sections designated as "dewetted" in Fig. 9. Although the boundaries are marked by distinct changes in contrast, both across and along the boundary (as discussed in the text), there is no resolvable evidence for a contiguous glassy film.

liquid-phase sintered polycrystalline materials.[8,9] Whether a boundary remains wetted by the liquid phase or not depends on the energy of the fully wetted boundary relative to that of a dry grain boundary. Generally, the boundary energy, whether "wet" or "dry," is expected to depend on both the relative misorientation across the boundary and on the orientation of the boundary (relative to a fixed frame of reference). For small angles of misorientation, where the boundary might be described by a low-density set of dislocations, the boundary energy is expected to be lower than one containing a glass interphase. Alternatively for large misorientations, the reverse is expected. At intermediate misorientations, portions of the boundary are expected to be either "wet" or "dry" depending on orientation. Also, over particular ranges of orientations, the boundary is expected to contain alternating, small segments of "wet" and "dry" boundary, analogous to a thermally facetted crystal surface.

The results of the present study provide a more comprehensive view of the structure of bicrystal boundaries in Al_2O_3. While these results provide extended verification to the energy-based theory of boundary structure,[8,9] they also reveal the need to modify or refine our understanding of the distinction between "wet" and "dry" boundaries. In particular, the present results have shown that for crystal misorientations, θ, of 12° or less, grain boundary dewetting occurs during boundary formation except for boundaries oriented close to the basal plane orientation in either crystal half. For small crystal misorientations, $\theta \leq 4°$, nonbasal oriented boundaries (Fig. 3) exhibit dislocation contrast and are not found to contain detectable traces of Si and Ca by EDS. For $\theta = 12°$, similar results apply to nonbasal oriented boundaries (Fig. 5). While nonbasal oriented portions of this 12° boundary appeared "dry," even when oriented close to $\{01\bar{1}2\}$ rhombohedral twin plane orientations, they did exhibit detectable concentrations of Si and Ca by EDS. Here, the retention of cations from the glass phase can be related to the enhanced lattice disorder and point defect concentration at the boundary that occurs with increased misorientation, much in the way that grain boundaries act as sinks for impurity segregation.

The present results also confirm the fact that bicrystal boundaries having a relatively large basal tilt component, i.e., $\theta \geq 7°$ about an axis normal to the *c*-direction, remain "wetted" for boundary orientations, ϕ, close to the median basal orientation. As seen in Fig. 5(b) (for $\theta = 12°$) and Fig. 8 (for $\theta = 7°$), these portions of the boundary contain a contiguous, glassy interphase, which is bounded primarily by basal surfaces. The present results on boundaries having a relatively large tilt component, θ, also confirm the fact that boundary orientations in the range of $\phi < \pm(\frac{1}{2})\theta$, about the medial basal plane orientation, are "missing" boundary orientations. Instead, the boundary plane abruptly changes orientation, such that adjacent, wetted boundary segments are aligned along the basal planes in either crystal half so that $\phi = +(\frac{1}{2})\theta$ or $\phi = -(\frac{1}{2})\theta$, as in Fig. 7(a). This change in boundary plane orientation relates to the fact that the combined energy plot for a wetted boundary exhibits cusps at positions corresponding to the basal orientations in the two crystals.[8,9] Similarly, the current results on a $\theta = 12°$ boundary (Fig. 6) also show that "dry" or dewetted portions of the boundary are inclined by roughly 30° or more to the fully wetted, basal portions of the boundary, as predicted.

The present study also examined the structure and composition of near basal-oriented boundaries, one corresponding to a small 3° basal plane tilt ($\theta = 3°$ about *a*), the other to 15° and 27° basal twists about the *c*-axis, with a small (<2°) basal tilt component. The results can be rationalized by the same combined energy approach, with only minor modification to the analysis. Results for these boundaries show little deviation in the expected periodicity normal to the basal planes and, thus, appear to be fully dewetted. These basal boundaries do, however, contain significant concentrations of Si and Ca, which, in comparison with off-boundary regions, are in excess of the equilibrium, impurity level concentrations in sapphire (estimated to be ≤250 ppm). In the absence of clear evidence for a glassy interphase, we conclude that Si and Ca cations from the glass phase are retained, preferentially on the basal planes. The retention of stable, excess concentrations of Si and Ca to basal boundaries, moreover, relates to the specific nature of basal defects, particularly basal faults that form on dewetting. Here, it is important to note that the basal stacking sequence of sapphire consists of 12 alternating layers of anions (O) and cations

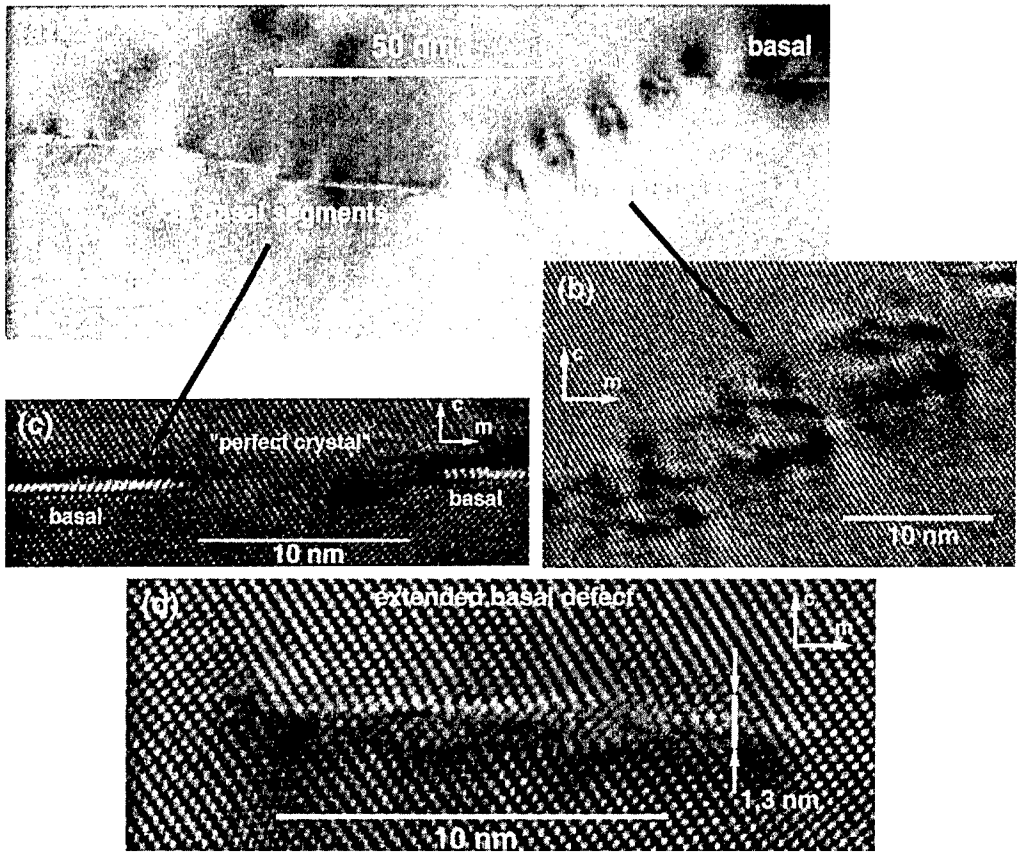

Fig. 11. TEM views of "steps" in the 3° basal tilt boundary also seen in Figs. 9 and 10. (a,b) For relatively large step heights, adjacent basal plane boundary sections are joined by a dislocation boundary segment, which is inclined by ~25° to the median basal plane orientation. (c) For smaller (~1 to 2 nm) step heights, adjacent basal plane segments are separated by regions of "perfect" crystal. (d) ***a***-axis HREM image of isolated basal plane boundary segment as seen in Figs. 10(a) and 10(b). Absence of interfacial glass film leads to conclusion that boundary contrast is due to dislocations and basal faults, which accommodate cation adsorbates from the glass phase.

(Al) and that, as originally noted by Kronberg,[10] basal fault energies contain relatively large "electrostatic" components, even when only next nearest neighbor configurations are altered. Basal fault energies, thus, are expected to be large, and, indeed, there have only been a few reports of dislocation dissociation on the basal planes in sapphire. Since the formation of a bicrystal boundary along the basal planes is likely to result in stacking errors, high-energy basal faults, which either are charged or contain relatively high densities of charge-compensating point defects, should be produced. The retention of secondary cations from the glass phase is expected to reduce the total energy of the basal faults and, thus, the boundary energy. This process is similar to the segregation of impurities to grain boundaries except that long-range diffusion of solute ions is not required. As a growth process forms the boundaries, as opposed to a deformation process, these fault-related considerations should also apply to basal twist boundaries. In the context of an energy-based theory of grain boundary structure,[8,9] the presence of Si and Ca reduces the otherwise high energy of basal-oriented "defect boundaries." Thus, for small basal tilt misorientations with or without a twist component, a "contaminated dry" boundary is energetically favored over either a "wetted" boundary or a "clean" boundary.

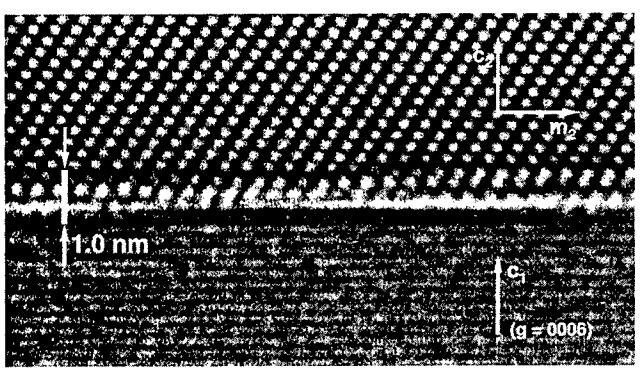

Fig. 12. HREM image from a 15° basal twist bicrystal boundary. In this cross-sectional view, the upper crystal half is aligned along an ***a***-axis and the bottom crystal half is imaged by 0006 lattice fringe contrast. Despite these inherent diffraction limitations, no significant change in expected periodic contrast is apparent across the boundary. Qualitatively similar results were also found for a nominally 30° basal twist boundary. In both cases, however, these twist boundaries were marked by detectable concentrations of Si and Ca, as boundary adsorbates.

Recent results by Gemmings *et al.*[11] lend support to this proposed effect of impurities on the energy of basal-oriented small angle boundaries. These authors made bicrystal boundaries by annealing two precisely aligned sapphire plates. For certain crystal misorientations and boundary orientations, the boundary assumed a facetted shape, portions of which were aligned parallel to the basal planes. After prolonged annealing, only the basal-oriented segments of boundary contained detectable excess concentrations of Si and Ca, originally present at impurity levels in the sapphire plates. This observation of preferential segregation strongly suggests that the energy of the basal boundary segments is relatively high, and is reduced by the segregation of Si and Ca.

In addition, a rationale for attachment of calcium and silicon to the basal plane of sapphire was suggested by Litton and Garofalini[12] and Blonski and Garofalini.[13] Using molecular dynamics simulations, these authors examined the atomic structure of sapphire basal surfaces in contact with glassy films of calcium aluminosilicate and calcium silicate. For calcium aluminosilicate films, their results predict that physical adsorption of Al, Si, and Ca cations from the glass phase occurs and results in the formation

of an ordered structure at the basal surface. Based on this result, complete desorption of Si and Ca from basal surfaces of sapphire is not expected to occur for most sintering conditions. The experimental results presented here are in agreement with this conclusion. Specifically, it has been shown that when bicrystal formation results in dewetting of the liquid phase, the basal-oriented portions of the boundary retain residual Si and Ca from the interphase. Moreover, even under conditions where complete dewetting has not occurred and the basal planes intersect the boundary, such as illustrated in Fig. 7(b), the presence of Si and Ca at basal growth ledges provides a reasonable explanation for the observed basal plane striations in image contrast along the boundary. In all cases, residual Si and Ca appears stabilized at the boundary by being incorporated within the boundary defect structure.

In a broader sense, the studies reported by Hansen and Phillips,[1] and Powell-Doğan and Heuer,[2] have led to the conclusions that most grain boundaries in vitreous-bonded aluminum oxide are wetted by glass and that only special boundaries, e.g., twin-related boundaries, are expected to be dry. Shaw and Duncombe[7] confirmed this finding by showing that roughly 84% of the boundaries in sintered alumina are penetrated by glass, leaving an estimated 16% of the boundaries intact. The present experiment examined only a small population of the infinite possibilities of grain boundary orientations between alumina grains. Also, without a complete evaluation of the Wulff shape and the grain boundary energy as a function of θ and ϕ, predictions beyond the narrow scope of small angle grain boundaries are chancy. Hence, a complete generalization of our results is not possible. Despite this, it appears that boundary dewetting is more general than suggested in the earlier studies. In our studies, dewetting occurred for basal twist-boundaries ($\theta = 15°$ and $\sim 30°$), for small angle tilt boundaries ($\theta \leq 3°$) of all boundary orientations and for larger tilt boundaries ($\theta \leq 12°$) having boundary orientations, ϕ, greater than $\sim 40°$ to the basal orientation. Therefore, dewetting of grain boundaries in aluminum oxide occurs over a range of boundary orientations and misorientations greater than would have been suspected from earlier studies. The results presented here are considered to be particularly applicable to a variety of materials having a high degree of directional texture.

V. Summary

In this study, oriented sapphire crystals grew through tapes of glass-bonded aluminum oxide producing sapphire bicrystal boundaries. Boundary misorientations, θ, included 3°, 7°, and 12° tilt boundaries obtained by rotations about a common ***a***-axis and 15° and 30° basal twist boundaries. The structure and composition of the boundaries depended on both the misorientations, θ, across the boundary and the relative orientation, ϕ, of the boundary within the bicrystal. Grain boundary dewetting was observed for all misorientation angles, θ, having tilt misorientations of 3° or less and for basal twist boundaries. Despite the occurrence of dewetting, small angle tilt and basal twist boundaries exhibited clear evidence for preferential adsorption of calcium and silicon at basal-oriented boundary sections. For larger tilt misorientations, $\theta = 7°$ and 12°, basal-oriented boundary segments were mostly completely wetted in that they contained a contiguous glass interphase; some basal boundary segments in the $\theta = 7°$ bicrystal, however, appeared to contain isolated, nanoscale pockets of glass phase. While boundary orientations for the $\theta = 7°$ boundary were limited to near-basal orientations, results from the $\theta = 12°$ boundary showed that dewetting occurred for all boundary orientations except the basal orientation. In agreement with earlier results,[8] the change from wetted, basal-oriented boundary to dewetted boundary was marked by an abrupt, 30° to 40° change in boundary orientation. Most of the results presented in this paper can be explained within the framework of the boundary energy theory.[8,9] A modification to this theory is suggested to account for the observation of "dry" basal boundaries containing residual Si and Ca from the liquid, glassy phase.

References

[1]S. C. Hansen and D. S. Phillips, "Grain Boundary Microstructures in a Liquid-Phase Sintered Alumina (α-Al_2O_3)," *Philos. Mag.*, **47**, 209–34 (1983).

[2]C. A. Powell-Doğan and A. H. Heuer, "Microstructure of 96% Alumina Ceramics: I, Characterization of the As-Sintered Materials," *J. Am. Ceram. Soc.*, **73** [12] 3670–76 (1990).

[3]D. S. Phillips and Y. R. Shiue, "Grain-Boundary Microstructures in Alumina Ceramics"; pp. 357–67 in Advances in Ceramics, Vol. 10, *Structure and Properties of MgO and Al_2O_3 Ceramics*. Edited by W. D. Kingery. American Ceramic Society, Columbus, OH, 1984.

[4]Y. Finkelstein, S. M. Wiederhorn, B. J. Hockey, C. A. Handwerker, and J. E. Blendell, "Migration of Sapphire Interfaces into Vitreous Bonded Aluminum Oxide"; pp. 258–79 in Ceramic Transactions, Vol. 7, *Sintering of Advanced Ceramics*. Edited by C. A. Handwerker, J. E. Blendell, and W. A. Kaysser. American Ceramic Society, Westerville, OH, 1990.

[5]J.-H. Choi, D.-Y. Kim, B. J. Hockey, S. M. Wiederhorn, C. A. Handwerker, J. E. Blendell, W. C. Carter, and A. R. Roosen, "Equilibrium Shape of Internal Cavities in Sapphire," *J. Am. Ceram. Soc.*, **80** [1] 62–68 (1997).

[6]P. L. Flaitz and J. A. Pask, "Penetration of Polycrystalline Alumina by Glass at High Temperatures," *J. Am. Ceram. Soc.*, **70** [7] 449–55 (1987).

[7]T. M. Shaw and P. R. Duncombe, "Forces between Aluminum Oxide Grains in a Silicate Melt and Their Effect on Grain Boundary Wetting," *J. Am. Ceram. Soc.*, **74** [10] 2495–505 (1991).

[8]D.-Y. Kim, S. M. Wiederhorn, B. J. Hockey, C. A. Handwerker, and J. E. Blendell, "Stability and Surface Energies of Wetted Grain Boundaries in Aluminum Oxide," *J. Am. Ceram. Soc.*, **77** [2] 444–53 (1994).

[9]J. E. Blendell, W. C. Carter, and C. A. Handwerker, "Faceting and Wetting Transitions of Anisotropic Interfaces and Grain Boundaries," *J. Am. Ceram. Soc.*, **82** [7] 1889–900 (1999).

[10]M. L. Kronberg, "Plastic Deformation of Single Crystals of Sapphire: Basal Slip and Twinning," *Acta Metall.*, **5**, 507–24 (1957).

[11]T. Gemming, S. Nufer, W. Kurtz, and M. Rühle, "Structure and Chemistry of Symmetrical Tilt Grain Boundaries in α-Al_2O_3: I, Bicrystals with 'Clean' Interface," *J. Am. Ceram Soc.*, **86** [4] 581–89 (2003).

[12]D. A. Litton and S. H. Garofalini, "Molecular Dynamics Simulations of Calcium Aluminosilicate Intergranular Films on (0001) Al_2O_3 Facets," *J. Am. Ceram. Soc.*, **83** [9] 2273–81 (2000).

[13]S. Blonski and S. H. Garofalini, "Atomistic Structure of Calcium Silicate Intergranular Films in Alumina Studied by Molecular Dynamics Simulations," *J. Am. Ceram. Soc.*, **80** [8] 1997–2004 (1997). □